Numerical Study of Heat Transfer Enhancement for a Flat Plate Solar Collector by Adding Metal Foam Blocks

Asst. Prof. Dr. Mohammed Abdulraouf Nima
Mechanical Engineering Department
College of Engineering- Baghdad University
E-mail: dralsafi@uobaghdad.edu.iq

Ali Mohammed Ali
Mechanical Engineering Department
College of Engineering- Baghdad University
E-mail: engali19927@gmail.com

ABSTRACT

Numerical study has been conducted to investigate the thermal performance enhancement of flat plate solar water collector by integrating the solar collector with metal foam blocks.The flow is assumed to be steady, incompressible and two dimensional in an inclined channel. The channel is provided with eight foam blocks manufactured form copper. The Brinkman-Forchheimer extended Darcy model is utilized to simulate the flow in the porous medium and the Navier-Stokes equation in the fluid region. The energy equation is used with local thermal equilibrium (LTE) assumption to simulate the thermofield inside the porous medium. The current investigation covers a range of solar radiation intensity at 09:00 AM, 12:00 PM, and 04:00 PM on the 8th of July 2016 under Iraq climate conditions, and a range of Reynolds number of ($207<Re<625$). The results show that the insertion of metal foam blocks caused a reduction in the absorber plate temperature and the possible enhancement in the heat transfer coefficient is more than 80% and as a result, the collector exhaust temperature will increase.
Keywords: Solar water collector, metal foam, finite volume method, Iraq climate.

دراسة عددية لتحسين الاداء الحراري لمجمع شمسي ذو الصفيحة المستوية بإضافة كتل من رغوة معدنية

أ.م.د. محمد عبد الرؤوف نعمة
قسم الهندسة الميكانيكية
كلية الهندسة– جامعة بغداد

علي محمد علي
قسم الهندسة الميكانيكية
كلية الهندسة– جامعة بغداد

الخلاصة

يقدم البحث الحالي دراسة نظرية لتحسين الاداء الحراري لمجمع شمسي مائي ذو الصفيحة المستوية حيث ان تحسين الاداء تم باضافة قطع من الرغوة المعدنية الى مصاعد المجمع الشمسي. تم فرض الجريان على انه مستقر, غير قابل للانضغاط, و ثنائي الابعاد يتدفق داخل مجرى مائل حاوي على ثماني قطع رغوة معدنية مصنوعة من النحاس. تم استخدام نموذج دارسي- برنكمان- فورشهايمر لمحاكاة الجريان في الوسط المسامي ومعادلة نـفْير ستوك في منطقة المائع و قد اختيرت معادلة الطاقة مع فرضية الاتزان الحراري (LTE) داخل الوسط المسامي. ان البحث الحالي يغطي عدة مديات للاشعاع الشمسي و المقاسة عند الساعة 09:00 ص, 12:00م, و 04:00م في الثامن من شهر يوليو لسنة 2016 تحت الضروف المناخية العراقية و لعدة مديات من رقم رينولد ($207<Re<625$). ان نتائج البحث الحالي اظهرت ان عملية اضافة الرغوة المعدنية قد تسببت بانخفاض درجة حرارة الصفيحة المستوية و تحسين معامل انتقال الحرارة بمقدار يصل الى اكثر من 80% وبسبب ذلك, تزداد درجة حرارة الماء الخارج من المجمع الشمسي.

الكلمات المفتاحية: مجمع شمسي مائي، رغوه معدنية، طريقة الحجم المحكوم، اجواء عراقية.

1. INTRODUCTION

At the present, crude oil is the main supplier of energy needed by the human, which is used in many applications, but the crude oil combustion releases emissions of carbon dioxide into environment and raises the environmental pollution. Extreme weather conditions and the continuous rising in the fuel price due to the scarcity of the crude oil forces us to deal with the valuable nature resources more effectively and research alternative green and non-depleted energy (renewable energy). Solar energy is one such option of the renewable energy which is represented by the solar radiation falling on the earth. The major component of any solar thermal system is the solar thermal collector where it used to transform the solar radiation into heat that carrying out of the collector by a working fluid (air, water or oil) passing through the collector. Flat plate solar water collectors are commonly used for low temperature applications below 100 ℃ such as residential applications, air conditioning (space heating), and industrial applications **Duffi**e and **Beckman**, **2013**. They are working in the recent 40~50 years without obvious changes in their design or operation principles **Iordanou, 2009**. The thermal performance enhancement for a flat plate solar collector may reduce its size and achieve higher exhaust temperature for extensive applications. To accomplish these purposes, many highly effective methods have been used in the previous research to improve the thermal performance including the methods of reducing the heat losses from the solar collector. There are two methods that used to reduce the heat losses from the solar collector, first method includes increasing the thermal resistance of the solar collector, such as using double or multi transparent cover, using evacuated tube receiver, using solar concentrators, using a V-grooved absorber, etc.

Second method includes a reduction in the temperature of the absorber. This is obtained by increasing the heat transfer coefficient inside the riser such as using twisted tapes installed inside the risers, improving the thermal properties of the working fluid due to the use of nanofluids, and using metal foam blocks as a porous medium partially or fully packed the risers which is used in the present research. A porous medium is considered as an effective enhancement method of heat transfer due to their intense mixing of the flow and their large surface area to volume ratio. Metal foams are a category of porous materials with unique properties that are utilized in heat transfer applications and several structural, **Ashby et al., 2000**. Metal foams are being produced as open-cell and closed-cell foams. Open-cell metal foam consists of pores that are open to their neighboring pores and allow the fluid to pass through them.

Extensive numerical and experimental studies had been conducted on the thermal enhancement in a flat plate solar collector or in channel. **Hadim, 1994** performed a numerical study to investigate the forced convection heat transfer in a channel partially and fully filled with porous medium and heated with localized heat sources that distributed at the lower wall. The extended Darcy model was utilized to describe the laminar flowfield inside the porous media and the energy equation with local thermal equilibrium condition (LTE) condition was utilized to describe the thermal performance within the porous media. Results showed that when the thermal conductivity ratio is unity, the heat transfer in both cases was almost the same, while the pressure drop was much lower in the case of partially filled channel. A numerical study was conducted by

Alkam and **Al-Nimr, 1999** to investigate the enhancement in the thermal performance of flat plate solar water collector by adding Aluminum foam substrates where it was formed as annular substrates and was installed at the inner wall of the risers. Their results showed that the addition of the Aluminum foam substrate enhance the heat transfer coefficient at the riser's wall, and thereby Nusselt number improved up to 27 times, but the inserting of the porous substrates led to increase the pressure drop up to 32 times. **Naphon, 2005** studied mathematically the thermal performance enhancement of flat-plate double pass air heater. The enhancement was achieved by inserting a porous medium into the lower duct (below the absorber). The thermal conductivity effect of the porous medium on the thermal performance was investigated. Results showed that the presence of the porous medium inside the solar air heater caused an increasing in the collector thermal efficiency by 25.9 %. A numerical study was obtained by **Bhargavi and Satyamurty, 2011** to establish the optimum arrangement and thickness of porous inserts in parallel plate channels subjected to a uniform heat flux at each plate in the case of forced convective heat transfer enhancement. The three different arrangements were: (1) a given porous substrate was attached to one wall (top or bottom), (2) two symmetric substrates were attached the walls, and (3) one porous substrate placed at the middle of the plates. The results showed that arrangement (3) yielded maximum enhancement in the Nusselt number due to the increasing of the flow velocity near the heated wall. **Chen and Huang, 2012** studied numerically the heat transfer enhancement in a channel of flat plate solar water collector by using an aluminum alloy foam blocks which were installed separately at the absorber. They found out that the presence of Aluminum foam blocks that partially filled the riser's channel had led to rise the mean Nusselt number up to 5 times. **Hwang et al., 2013** investigated the effect of pulsating flow in flat plate solar water collector that was enhanced by adding metal foam blocks. To simulate thermo field, they used two transient energy equations for solid and fluid phase based on (LTNE) condition. Their findings showed that the total cycle-space averaged heat transfer enhancement factor (Nu_m/Nu_{m-non}) increased with Reynolds number, effective thermal conductivity ratio and pulsating amplitude where it reached to 6 as a maximum value that existed during the tests and thereby, the pulsating flow gave further enhancement than the steady flow. An experimental study was conducted by **Ranjithkumar et al., 2015** to examine the benefit of the integration of flat-plate solar air heater by a porous medium. The porous media that was used in their study were black stone and sand stone where they were utilized as a heat storage material. Their results showed that the addition of porous medium led to increase the efficiency of the air heater up to 77%. An experimental study was conducted by **Abbas, 2016** to investigate the heat transfer improvement in a constant heat flux heated channel partially filled with copper foam blocks with air as the working fluid. The effect of several parameters such as Reynolds number ($638 \leq Re \leq 2168$), heat flux ($453 \leq q \leq 4462$ W/m^2), pores per inch PPI (10, 40), and Darcy number ($1.77\times10^{-5} \geq Da \geq 3.95\times10^{-6}$) on the heat transfer performance were studied. Results show that the heat transfer performance was increased by 85% for all studied cases where the enhancement in the heat transfer was recognized by the comparison between the porous and non-porous channel.

In the present study, mixed convection heat transfer in an inclined channel that supplied with metal foam (copper foam) blocks and exposed to a constant heat flux, is numerically examined with water as the working fluid. The influence of heat flux (solar radiation), and Reynolds

number variation on isotherms, streamlines, and the heat transfer rate at the heated wall (absorber plate) in terms of local and mean heat transfer coefficient are investigated and analysed.

2. MATHEMATICAL FORMULATION

2.1 Geometry and Coordinate System

A schematic representation of the system under investigation is shown in **Fig.1**. A two dimensional model in cartesian coordinate system is used to describe the problem of steady mixed convection heat transfer in an inclined channel with an angle (γ) from the horizontal position. The channel is partially filled with discrete porous blocks and heated uniformly from the top wall (absorber plate) by the solar radiation, while the bottom wall is insulated. Both walls (upper and lower) are impermeable and rigid.

2.2 Assumptions

To solve the flow and heat transfer equations (conservation of mass, momentum and energy) some assumptions should be made to simplify the problem:

1. Steady state, laminar and incompressible flow.
2. The numerical study is in two dimensions(x-y).
3. There is no heat generation or dissipation.
4. The porous medium is rigid, uniform, isotropic and fully saturated with water.
5. Thermophysical properties of the both phases (solid and fluid) are assumed constant.
6. The effect of buoyancy is considered and Boussinesque's approximation is invoked.
7. The computational domain is large enough than the physical domain to verify exit conditions ($l > L$) [see **Fig.3**].

2.3 Governing Equations

In this study, the Navier-Stokes equation is introduced to describe the flowfeild in the clear fluid region while the Brinkman-Forchheimer extended Darcy model is introduced to describe the flowfeild inside the porous medium. To model the thermofield inside the porous medium, the local thermal equilibrium (LTE) is used in between the solid and fluid phases. The above mentioned equations are expressed as follow, **Chen and Huang, 2012**:

- **Conservation of mass**

$$\frac{\partial u}{\partial x}+\frac{\partial v}{\partial y}=0 \tag{1}$$

- **Conservation of Momentum**

In the clear fluid region:

$$u\frac{\partial u}{\partial x}+v\frac{\partial u}{\partial y}=-\frac{1}{\rho_f}\frac{\partial P}{\partial x}+\upsilon_{eff}\left(\frac{\partial^2 u}{\partial x^2}+\frac{\partial^2 u}{\partial y^2}\right)+\mathrm{g}sin(\gamma)\beta(T-T_i) \quad \text{[x-axis]} \tag{2}$$

$$u\frac{\partial v}{\partial x}+v\frac{\partial v}{\partial y}=-\frac{1}{\rho_f}\frac{\partial P}{\partial y}+\upsilon_{eff}\left(\frac{\partial^2 v}{\partial x^2}+\frac{\partial^2 v}{\partial y^2}\right)+\mathrm{g}cos(\gamma)\beta(T-T_i) \quad \text{[y-axis]} \tag{3}$$

In the porous medium:

$$\frac{1}{\varepsilon^2}\left[u\frac{\partial u}{\partial x}+v\frac{\partial u}{\partial y}\right]=\frac{-1}{\rho_f}\frac{\partial P}{\partial x}+\frac{1}{\varepsilon^2}\upsilon_{eff}\left(\frac{\partial^2 u}{\partial x^2}+\frac{\partial^2 u}{\partial y^2}\right)-\left[\frac{\upsilon_f}{K}+\frac{\varepsilon C}{\sqrt{K}}\left|\vec{V}\right|\right]u+\mathrm{g}sin(\gamma)\beta(T-T_i) \quad \text{[x-axis]} \tag{4}$$

$$\frac{1}{\varepsilon^2}\left[u\frac{\partial v}{\partial x}+v\frac{\partial v}{\partial y}\right]=\frac{-1}{\rho_f}\frac{\partial P}{\partial y}+\frac{1}{\varepsilon^2}\upsilon_{eff}\left(\frac{\partial^2 v}{\partial x^2}+\frac{\partial^2 v}{\partial y^2}\right)-\left[\frac{\upsilon_f}{K}+\frac{\varepsilon C}{\sqrt{K}}\left|\vec{V}\right|\right]v+\mathrm{g}cos(\gamma)\beta(T-T_i)\text{ [y-axis] (5)}$$

- **Conservation of energy**

In the clear fluid region:

$$u\frac{\partial T}{\partial x}+v\frac{\partial T}{\partial y}=\frac{k_f}{(\rho C_p)_f}\left(\frac{\partial^2 T}{\partial x^2}+\frac{\partial^2 T}{\partial y^2}\right) \quad (6)$$

In the porous medium:

$$u\frac{\partial T}{\partial x}+v\frac{\partial T}{\partial y}=\frac{k_{eff}}{(\rho C_p)_f}\left(\frac{\partial^2 T}{\partial x^2}+\frac{\partial^2 T}{\partial y^2}\right) \quad (7)$$

In Eqs. (4) and (5), the third term on the R.H.S can be defined as a resistance term produced by porous medium in the flowfield. The term consists of two part, the first part knowing as Darcy term which represents the pressure drop due to the viscous friction at the interface between fluid and solid phases, the second part knowing as Forchheimer term which represents the pressure drop due to the drag and the flow separation which may take place at higher Reynolds number, **Began, 2006.**

The above set of equations are semi-empirical equations since the equations which govern the relevant empirical coefficients, such as k_{eff}(the effective thermal conductivity, K(permability) and C(inertial parameter) are came from experimental tests and these coefficients do not have a universal value, **Chen and Huang, 2012**.

To estimate the effective thermal conductivity of open-cell metal foam, k_{eff}, the following correlation was proposed by **Calmidi and Mahajan, 1999** as;

$$k_{eff}=\varepsilon k_f+0.195(1-\varepsilon)^{0.763}\,k_s \quad (8)$$

Where the fluid (water) thermal conductivity k_f is taken as 0.603 W/m.K and thermal conductivity of the copper foams k_s (386 W/m.K), **Holman, 2010**. The effective thermal conductivity of the metal foam is found to be equal to (13.2349 W/m.K).

2.4 Boundary Conditions

To complete the formulation of the intended problem, some boundary conditions must be introduced:

- At the channel inlet: $x=0,\ 0\le y\le H \Rightarrow u=u_i$, $v=0$, $P=P_i$, and $T=T_i$
- At the channel exit: $x=l,\ 0<y<H \Rightarrow \frac{\partial u}{\partial x}=0, \frac{\partial v}{\partial x}=0$, and $\frac{\partial T}{\partial x}=0$
- At the lower wall: $y=0,\ 0<x<l \Rightarrow u=v=0, \frac{\partial P}{\partial x}=\mu\frac{\partial^2 u}{\partial y^2}$ and $\frac{\partial T}{\partial y}=0$
- At the upper wall:

$0<x<l, y=H \Rightarrow u=0, v=0, \frac{\partial P}{\partial x}=\mu\frac{\partial^2 u}{\partial y^2}$ and

$$\frac{\partial T}{\partial y} = \begin{cases} -\frac{q_{ab}}{k_{eff}} & \text{over the porous blocks} \\ -\frac{q_{ab}}{k_f} & \text{clear fluid heated region with } x \le L \\ 0 & x > L \end{cases}$$

2.5 Nondimensionalization of the Governing Equations.

The existence of the pressure term in the momentum equation causes a difficulties in the numerical solution, this leads to resort to the Stream Function-Vorticity method which deals with the elimination of the pressure term from the momentum equation by some mathematical manipulations, **Patenkar, 1980.** To nondimensionalize the variables used in the governing equations, the following dimensionless variables are defined by, **Chen and Huang, 2012** where (*) referees to dimensionless value;

$$Re_f = \frac{u_i D_h}{\upsilon_f}, Re_{eff} = \frac{u_i D_h}{\upsilon_{eff}}, Pr_f = \frac{\upsilon_f}{\alpha_f}, Pe_f = \frac{u_i D_h}{\alpha_f} = Re_f Pr_f \quad Gr = \frac{g\beta \frac{q_{ab}}{K_f} {D_h}^4}{{\upsilon_f}^2}, Ri = \frac{Gr}{Re^2}$$

$$\alpha_f = \frac{k_f}{\rho Cp}, Da = \frac{K}{{D_h}^2}, \lambda = \frac{k_{eff}}{k_f}, x^* = \frac{x}{D_h}, y^* = \frac{y}{D_h}, L^* = \frac{L}{D_h}, l^* = \frac{l}{D_h}, w^* = \frac{w}{D_h}, s^* = \frac{s}{D_h}$$

$$P^* = \frac{P}{\rho {u_i}^2}, T^* = \frac{T - T_i}{\frac{q_{ab} D_h}{k_f}} \quad u^* = \frac{u}{u_i}, v^* = \frac{v}{u_i}, \left|\vec{V}^*\right| = \sqrt{{u^*}^2 + {v^*}^2}, \Psi^* = \frac{\Psi}{u_i D_h}, \omega^* = \frac{\omega D_h}{u_i}$$

Now, the resulting governing equations in non-dimensional form are shown below:

$$\frac{\partial^2 \Psi^*}{\partial {x^*}^2} + \frac{\partial^2 \Psi^*}{\partial {y^*}^2} = -\omega^* \tag{9}$$

In the clear fluid region:

$$u^* \frac{\partial \omega^*}{\partial x^*} + v^* \frac{\partial \omega^*}{\partial y^*} = \frac{1}{Re_f}\left[\frac{\partial^2 \omega^*}{\partial {x^*}^2} + \frac{\partial^2 \omega^*}{\partial {y^*}^2}\right] + Ri\left(\cos(\gamma)\frac{\partial T^*}{\partial x^*} - \sin(\gamma)\frac{\partial T^*}{\partial y^*}\right)$$

(10)

$$u^* \frac{\partial T^*}{\partial x^*} + v^* \frac{\partial T^*}{\partial y^*} = \frac{1}{Pe_f}\left[\frac{\partial^2 T^*}{\partial {x^*}^2} + \frac{\partial^2 T^*}{\partial {y^*}^2}\right] \tag{11}$$

The pressure distribution in the clear fluid region can be expressed as follow:

$$\frac{\partial^2 P^*}{\partial {x^*}^2} + \frac{\partial^2 P^*}{\partial {y^*}^2} = 2\left(\frac{\partial u^*}{\partial x^*}\frac{\partial v^*}{\partial y^*} - \frac{\partial v^*}{\partial x^*}\frac{\partial u^*}{\partial y^*}\right) - Ri\left(sin(\gamma)\frac{\partial T^*}{\partial x^*} + sin(\gamma)\frac{\partial T^*}{\partial y^*}\right) \tag{12}$$

In the porous medium:

$$u^* \frac{\partial \omega^*}{\partial x^*} + v^* \frac{\partial \omega^*}{\partial y^*} = \frac{1}{Re_{eff}}\left[\frac{\partial^2 \omega^*}{\partial {x^*}^2} + \frac{\partial^2 \omega^*}{\partial {y^*}^2}\right] + Ri\left(\cos(\gamma)\frac{\partial T^*}{\partial x^*} - \sin(\gamma)\frac{\partial T^*}{\partial y^*}\right) - \frac{\varepsilon^2}{\mathrm{Re\ Da}}\omega^* - \frac{\mathrm{C}\,\varepsilon^3}{\sqrt{\mathrm{Da}}}\left|\bar{V}\right|\omega^* - \frac{\mathrm{C}\,\varepsilon^3}{\sqrt{\mathrm{Da}}}\left[v^*\frac{\partial|\bar{V}|}{\partial x^*} - u^*\frac{\partial|\bar{V}|}{\partial y^*}\right] \tag{13}$$

$$u^* \frac{\partial T^*}{\partial x^*} + v^* \frac{\partial T^*}{\partial y^*} = \frac{\lambda}{Pe_f}\left[\frac{\partial^2 T^*}{\partial {x^*}^2} + \frac{\partial^2 T^*}{\partial {y^*}^2}\right] \tag{14}$$

And the pressure distribution in the porous medium can be defined as follow:

$$\frac{\partial^2 P^*}{\partial {x^*}^2} + \frac{\partial^2 P^*}{\partial {y^*}^2} = 2\left(\frac{\partial u^*}{\partial x^*}\frac{\partial v^*}{\partial y^*} - \frac{\partial v^*}{\partial x^*}\frac{\partial u^*}{\partial y^*}\right) - Ri\left(\sin(\gamma)\frac{\partial T^*}{\partial x^*} + \sin(\gamma)\frac{\partial T^*}{\partial y^*}\right) + \frac{\varepsilon^3 C}{\sqrt{Da}}\left(u^*\frac{\partial|\overrightarrow{V^*}|}{\partial x^*} + v^*\frac{\partial|\overrightarrow{V^*}|}{\partial y^*}\right)$$

(15)

Where: $u^* = \frac{\partial \Psi^*}{\partial y^*}$, $v^* = -\frac{\partial \Psi^*}{\partial x^*}$, $\left|\overrightarrow{V^*}\right| = \sqrt[2]{u^{*2} + v^{*2}}$ (16)

The dimensionless boundary conditions will be:

❖ At the channel inlet:

$x^* = 0, 0 < y^* < 1 \Rightarrow u^* = 1, v^* = 0, \Psi^* = y^*, \omega^* = 0, P^* = P_i{}^*, \ T^* = 0$

❖ At the channel exit:

$x^* = l^*, 0 < y^* < 1 \Rightarrow \frac{\partial u^*}{\partial x^*} = 0, \frac{\partial v^*}{\partial x^*} = 0, \frac{\partial T^*}{\partial x^*} = 0, \frac{\partial \omega^*}{\partial x^*} = 0, \frac{\partial^2 \Psi^*}{\partial x^{*2}} = 0$

❖ At the lower wall:

$y^* = 0, \ 0 < x^* < l^* \Rightarrow u^* = 0, v^* = 0, \Psi^* = 0, \omega^* = -\frac{\partial^2 \Psi^*}{\partial y^{*2}}, \frac{\partial T^*}{\partial y^*} = 0, \ \frac{\partial P^*}{\partial x^*} = \frac{-1}{Re} \frac{\partial \omega^*}{\partial y^*}$

❖ At the upper wall:

$y^* = 1, \ 0 < x^* < l^* \Rightarrow u^* = 0, v^* = 0, \Psi^* = 1, \ \omega^* = -\frac{\partial^2 \Psi^*}{\partial y^{*2}},$

$\frac{\partial P^*}{\partial x^*} = \frac{-1}{Re} \frac{\partial \omega^*}{\partial y^*}$, $\frac{\partial T^*}{\partial y^*} = \begin{cases} -\frac{1}{\lambda} & \text{over the porous blocks} \\ -1 & \text{clear fluid heated region } (x^* \le L^*) \\ 0 & x^* > L^* \end{cases}$

❖ **Fluid-Porous Interface Condition**

At the fluid-porous interface, the continuity of velocity components, temperature, stresses, and heat flux are valid, **Fu et al., 1996**.

$u_{por}{}^* = u_f{}^*, v_{por}{}^* = v_f{}^*, \Psi_{por}{}^* = \Psi_f{}^*, \omega_{por}{}^* = \omega_f{}^*$

$\frac{\partial v^*{}_f}{\partial x^*} = \frac{\mu_{eff.}}{\mu_f} \left[\frac{\partial v^*{}_{por}}{\partial x^*}\right], \left[\frac{\partial u^*{}_f}{\partial x^*} + \frac{\partial v^*{}_f}{\partial y^*}\right] = \frac{\mu_{eff.}}{\mu_f} \left[\frac{\partial u^*{}_{por}}{\partial x^*} + \frac{\partial v^*{}_{por}}{\partial y^*}\right]$

$T_{por}{}^* = T_f{}^*, \frac{\partial T^*{}_f}{\partial x^*} = \lambda \frac{\partial T^*{}_{por}}{\partial x^*}, \Psi_{por}{}^* = \Psi_f{}^*, \ \frac{\partial \Psi_{por}{}^*}{\partial x^*} = \frac{\partial \Psi_f{}^*}{\partial x^*}$; $\omega_{por}{}^* = \omega_f{}^*$, $\frac{\partial \omega_{por}{}^*}{\partial x^*} = \frac{\partial \omega_f{}^*}{\partial x^*}$

2.6 Further Calculations

2.6.1 The Nusselt Number and Heat Transfer Coefficient

The local heat transfer coefficient and Nusselt number can be defined as, **Began, 2006.**

$\mathrm{h}_x = \frac{q_{ab}}{(T_w - T_b)_x}$, $\mathrm{Nu}_x = \frac{\mathrm{h}_x \, \mathrm{D}_h}{k_f} = \frac{\frac{q_{ab} \mathrm{D}_h}{k_f}}{(T_w - T_b)_x} = \frac{1}{T_w{}^* - T_b{}^*}$ (17)

Where $T_w{}^*$ is the dimensionless wall temperature and $T_b{}^*$ is the dimensionless bulk temperature and can be defined as:

$T_b{}^* = \frac{\int_0^1 T^* u^* \, \mathrm{d}y^*}{\int_0^1 u^* \mathrm{d}y^*}$ (18)

The mean heat transfer coefficient is calculated as follows:

$$h_m = \frac{1}{L^*}\int_0^{L^*} h_x \, dx^* \quad (19)$$

The above integration is obtained over the physical domain.

3. NUMERICAL PROCEDURE

Numerical methods represent a useful alternative to analytical solutions. Such methods have proven to be increasingly popular. In the present work, the velocity and pressure fields in Eqs. (2) to (5) are treated by the Stream Function-Vorticity method of **Patanker, 1980**. The obtained system of equations included the energy equation [Eqs. (9) to (15)], is then solved by a fully implicit control volume-based on finite difference formulation with the use of up-wind differencing scheme of **Patanker, 1980**, to discretize the combined convective and conductive terms. A line-by-line tri-diagonal matrix algorithm TDMA is utilized to solve the system of algebraic equations that extracted from the discretization process of the differential governing equations. A computer program was build using MATLAB R2013a to implement the above procedure and to solve the governing equations. A relative error less than 10^{-5} is required for the temperature fields between successive iterations (for the mean Nusselt number). The flow chart of the built computer program is shown in **Fig.3**.

Before proceeding further, the grid independency test is performed first. Numerical tests are carried out for various grid size shown in **Fig.2**. It is observed that the mean Nusselt number values for a grid size larger than 691x 55 dose not vary more than 1.9%. Therefore, a grid size of 691x 55 is chosen for further computation because it consumed less computing time. A non-uniform grid system is used in the x-direction to provide a fine grid generation inside the metal foam blocks as shown in **Fig.1.** A relative error less than 10^{-5} is required for both the velocity and temperature fields between successive iterations (for the mean Nusselt number), and the normalized residual for the pressure field are less than 10^{-7} to achieve convergence.

$$\bar{R} = \frac{\sum|a_E\phi_E + a_W\phi_W + a_N\phi_N + a_S\phi_S + b - a_P\phi_P|}{\sum|a_P\phi_P|} \leq 10^{-7} \quad (20)$$

4. CODE VALIDATION

The present program codes are validated with the numerical results of **Hadim, 1994** where his work utilized the vorticity and stream function analysis and used the finite volume method in the discretization process of the governing equations. The numerical solution was obtained on a porous medium with (ε=0.97, C=0.1, Da=10^{-3}, Pr=10, Re=250) partially and fully filled a horizontal channel as shown in **Fig.4**. It can be seen from **Fig.5** that the present program results are made a good agreement with **Hadim, 1994**.

5. RESULTS AND DISCUSSION

In the present study, the problem of mixed convection heat transfer through an inclined channel integrated with metal foam blocks that subjected to constant heat flux, is solved based on local thermal equilibrium model. Numerical computations were performed for an inclined channel of 0.02 m height, 1.8 m length, and 23^o tilted angle for July, **Camelia and Dorin, 2014**. The channel is provided with eight (2 cm height, 3 cm thickness) foam blocks that made by

copper with porosity of $\varepsilon = 0.903$, inertial coefficient $C = 0.17$, permeability K= 7.85×10^{-8}, pore per inch=10 PPI, thermal conductivity ratio $\lambda = 21.25$ with water as a working fluid of $Pr = 5.885$.

The numerical results are presented by the pressure drop, temperature distribution, stream lines, and local and mean heat transfer coefficients.

5.1 Pressure Drop

The effect of inserting metal foam blocks on the pressure distribution along the channel is demonstrated in **Fig.6**. It is obvious that the pressure drop in the case of metal foam insertion is much greater than that in the fluid case. This is due to the permeability of the metal foam and the tortuous paths inside the porous structure. Also, it can be noticed form **Fig.6** that the pressure has been dropped linearly through the metal foam blocks. This is can be attributed to the low value of fluid velocity throughout the channel.

5.2 Temperature Distribution

In general, the presence of metal foam blocks caused to discretize the growth of thermal boundary layer along the channel. In addition, the growth of subsequent thermal boundary layer after each metal foam block is retreated due to the disturbance which arising from the fluid flowing through the metal foam blocks.

The effect of metal foam insertion (MFI) on the temperature contours along the channel is shown in **Figs.7**, **8**, **9**, and **Fig.10**. The temperature contours show that when metal foam blocks are added, a great reduction in the wall temperature value is observed that a companied with a noticeable increase in the working fluid temperature. The overall heat transfer processes are improved by the inserting of metal foam blocks where part of heat is transferred from the heat source by means of conduction through the solid matrix and the other part is transferred by means of convection to the incoming fluid that passed through the metal foam blocks.

Fig.7 and **Fig.8** show the influence of solar radiation intensity variation on the temperature contours along the channel without and with metal foam insertion, respectively. The value of solar radiation intensity has been taken for different time at 12:00 PM (938 W/m^2) and 04:00 PM (515 W/m^2) on the 7th of July. It can be seen that the impact of solar radiation intensity change is unclear with respect to the temperature contours along the channel. This is due to the working fluid nature and the limitation of the solar radiation intensity.

Fig.9 and **Fig.10** show the effect of Reynolds number variation on the thermal boundary layer growth for $Gr = 4.5 \times 10^5$ (I=649 W/m^2). It is obvious that the temperature is inversely proportional with the Reynolds number values. The retreat in the growth of thermal boundary layer was a consequence of increasing Reynolds number.

5.3 Streamlines

The effect of metal foam insertion (MFI) on the streamlines along the channel is shown in **Figs.11, 12**, **13**, and **Fig.14**. It can be noticed that the distortion of streamlines becomes more pronounced in the case of metal foam insertion in comparing with the clear fluid case.

Fig.11 and **Fig.12** show the effect of solar radiation intensity variation on the streamlines along the channel. It shows the deviation of streamlines in the opposite direction of gravity and

this deviation is increased as the fluid flows further through the channel. This is due to the increasing of buoyancy effect as the fluid temperature is increased. The Grashof number variation is diminished in the case of channel with metal foam blocks, due to the distortion that existed by the presence of the foam blocks, the working fluid nature, and the low value of the solar radiation intensity.

Fig.13 and **Fig.14** present the effect of Reynolds number variation on the streamlines for $Gr = 4.5 \times 10^5$. It shows that the Reynolds number increase has an inverse influence on the streamlines deviation because of higher inertia effect and low fluid temperature gradient.

5.4 Local and Mean Heat Transfer Coefficient

The effect of inserting metal foam blocks on the heat transfer coefficient is presented in **Figs.15**, and **16**. It can be seen that the local heat transfer coefficient in the case of channel with metal foam insertion is higher than the clear fluid case as the thermal boundary layer has faded through the metal foam blocks. The expected enhancement that obtained by metal foam integration had been checked based on the enhancement in mean heat transfer coefficient that given in Eq. (19). The ratio of the mean heat transfer coefficient with metal foam to that without metal foam ranges from 1.8 to 2.3 as shown in **Fig.16**. The obtained enhancement result was adapted in the design consideration for choosing the riser's length.

Fig.17 and **Fig.18** show the influence of solar radiation intensity variation on the heat transfer coefficient for both cases (with and without metal foam insertion). It can be noticed that the heat transfer coefficient was not affected by the change of solar radiation intensity in the case of channel with metal foam insertion. But, it changed slightly in the clear fluid case where it increased as the solar radiation intensity increased. This is due to the buoyancy effect which caused an increasing in the fluid velocity near the heated wall.

Fig.19 and **Fig.20** show the effect of Reynolds number variation on the heat transfer coefficient for both cases (with and without metal foam insertion). It can be seen that the heat transfer coefficient is directly proportional to the Reynolds number for the same Grashof number value. This increase in Reynolds number causes a reduction in the thermal boundary layer thickness with the domination of the incoming cold fluid and larger fluid mixing which increases the heat transfer coefficient.

6. Conclusions

1- The fluid temperature for the case of inserting metal foam blocks is greater than that in the case of without metal foam blocks (fluid case).
2- The variation of the heat flux has lower effect on the heat transfer characteristics for the channel with metal foam insertion.
3- The local and mean heat transfer coefficient increases with the increase of the Reynolds number.
4- The enhancement in the mean heat transfer coefficient for the case of metal foam insertion is found to be more than 80% in comparison with that of the fluid case.
5- The insertion of metal foam blocks caused an increasing in the pressure drop.

REFERENCES

- Abbas H. Hajeej, 2016, *Experimental Investigation of Convection Heat Transfer Enhancement in Horizontal Channel Provided with Metal Foam Blocks*, University of Baghdad, Journal of Engineering, Vol.22, No.5, PP.144-161.
- Ashby, M.F., Evans, A.G., Fleck, N.A., Gibson, L.J., Hutchinson, J.W. and Wadley, H.N.G., 2000, *Metal Foams: a Design Guide*, Butterworth-Heinemann, Boston, MA.
- Calmidi, V.V., and Mahajan, R.L.,1999, *The effective Thermal Conductivity of High Porosity Metal Foams*, ASME Journal of Heat Transfer, Vol. 121, PP. 466–471.
- Camelia Stanciu, and Dorin Stanciu, 2014, *Optimum tilt angle for flat plate collectors all over the world*, International Journal of Heat and Mass Transfer, Vol. 81, PP. 133–134.
- Chih-Cheng Chen, and Po-Chuan Huang, 2012, *Numerical study of heat transfer enhancement for a novel flat-plate solar water collector using metal-foam blocks*, International Journal of Heat and Mass Transfer, Vol.81, PP. 6734–6756.
- D. Bhargavi and V.V. Satyamurty, 2011, *Optimum Porous Insert Configuration for Enhanced Heat Transfer in Channels*, Journal of Porous Medium, Vol. 14, No. 3, PP.187-203.
- Duffie, J.A., Beckman, W. A, *Solar Engineering of Thermal Process*, Wiley Interscience Publications, John Wiley & Sons, New York (2013).
- Wu-Shung Fu, Hsin-Chien Huang, and Wei-Yan Liou, 1996, *Thermal enhancement in laminar channel flow with a porous block*, International Journal of Heat and Mass Transfer, Vol. 39, No. 10, PP.2165-2175.
- G. Iordanou, 2009, *Flat-plate solar collectors for water heating with improved heat transfer for application in climatic conditions of the Mediterranean region*, Ph.D. Thesis, University of Durham.
- Hadim A. 1994, *Forced convection in a porous channel with localized heat sources*, ASME, Journal of Heat Transfer; Vol.116, PP.465–471.
- Holman J. P.,"Heat Transfer, 10th Edition", McGraw-Hill Higher Education, (2010).
- M. K. Al-Nimar, and M. k. Alkam, 1999, *Solar Collectors with Tubes Partially Filled with Porous Substrate*, ASME, Journal of Solar Engineering, Vol. 121, PP.20-24.
- Nield D. A., and Bejan A., *Convection in Porous Media*, New York, Springer, (2006).
- Paisarn Naphon, 2005, *Effect of Porous Medium on Thermal Performance of the Double-Pass Flat Plate Solar Air Heater*, International Journal of Heat and Mass Transfer, Vol. 32, PP. 140-150.
- Suhas V. Patankar, *Numerical heat transfer and fluid flow*, New York: McGraw-Hill; (1980).
- Po-Chuan Huang, Chih-Cheng Chen, and Hsiu-Ying Hwang, 2013, *Thermal enhancement in a flat-plate solar water collector by flow pulsation and metal-foam blocks*, International Journal of Heat and Mass Transfer, Vol. 61, PP.696–720.
- Ranjithkumar K., Pradeep Kumar S. L., and Jayaprakash L., 2015, *Design and Thermal Analysis of Solar Plate Collector with and without Porous Medium*, International Journal of Innovative Research in Science Engineering and Technology, Vol.4, No.2, PP. 447-457.

NOMENCLATURE

C= inertia coefficient.
C_p=specific heat at constant pressure, J/kg.K.
Da= Darcy number.
D_h = Hydraulic diameter (D_h=H), m.
g = gravitational acceleration, m/s^2.
Gr = Grashof number.
H = channel height, m.
h = local heat transfer coefficient, W/m^2.K.
I = Solar radiation intensity, W/m^2.
k = thermal conductivity, W/m .K.
L = Risers length (length of the physical domain), m.
l = Length of the computational domain, m.
Nu = Nusselt number.
p = pressure, pa.
Pr = Prandtl Number.
q = heat flux, W/m^2.
Re= Reynolds number.
Ri= Richardson number.
K = permeability of the porous medium, m^2.
s = porous block spacing, m.
T = temperature, °C.
u = axial velocity, m/s.
v = transverse velocity, m/s.
w = width of the copper foam block, m.

Greek Symbols

ν = kinematic viscosity, m^2/s.
β = thermal expansion coefficient, 1/K
ε = porosity.
μ = dynamic viscosity, kg m/s.
ρ = density of water, kg/m^3.
λ = Thermal conductivity ratio
γ = Collector inclination angle, ^{o}
ω = vorticity, 1/s
Ψ = Stream-function, m^2/s

Subscripts

ab = absorbed.
eff = effective.
f = fluid.
i = inlet.
m = mean.

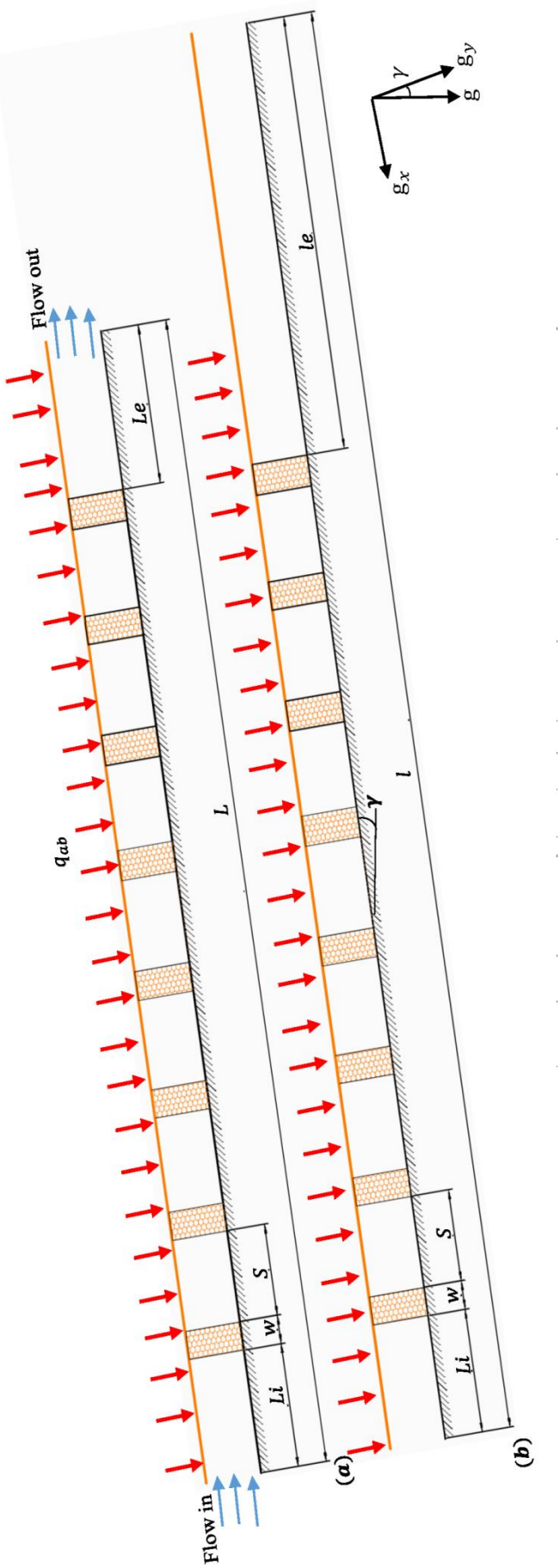

Figure 1. (a) Schematic Diagram of the Physical Domain, **(b)** Schematic Diagram of the Computational Domain.

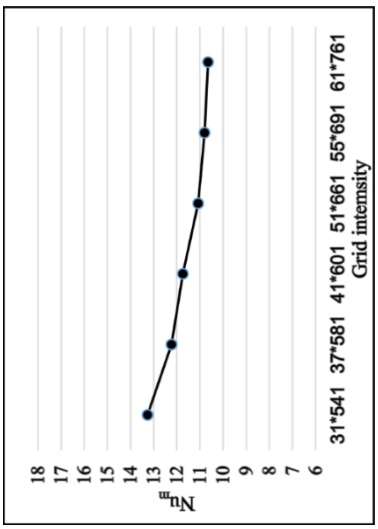

Figure 2. Grid Independency Curve.

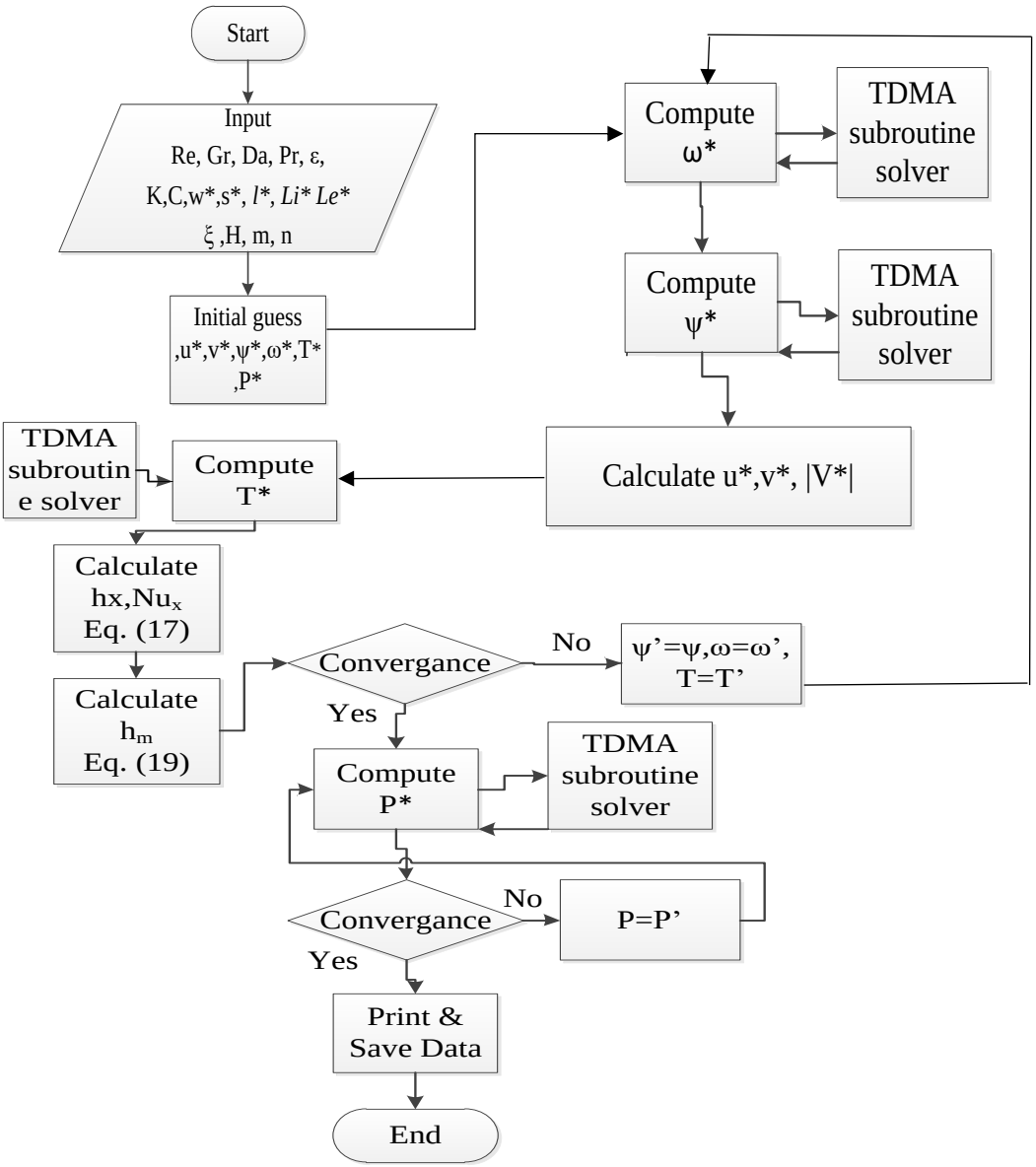

Figure 3. Flow Chart for the Computer Program.

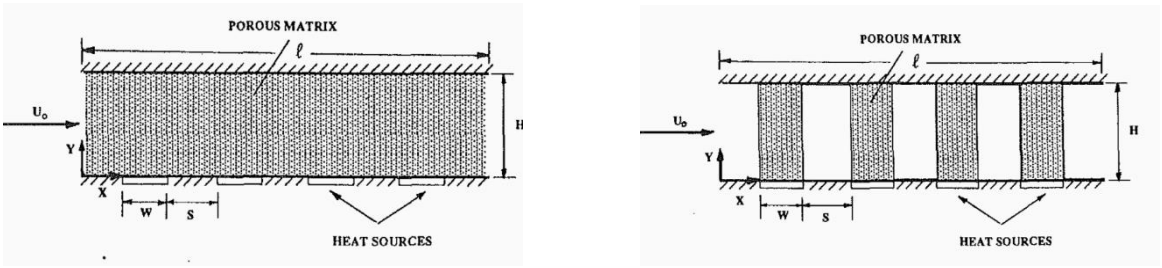

Figure 4. Physical Domain studied by **(Hadim, 1994)**.

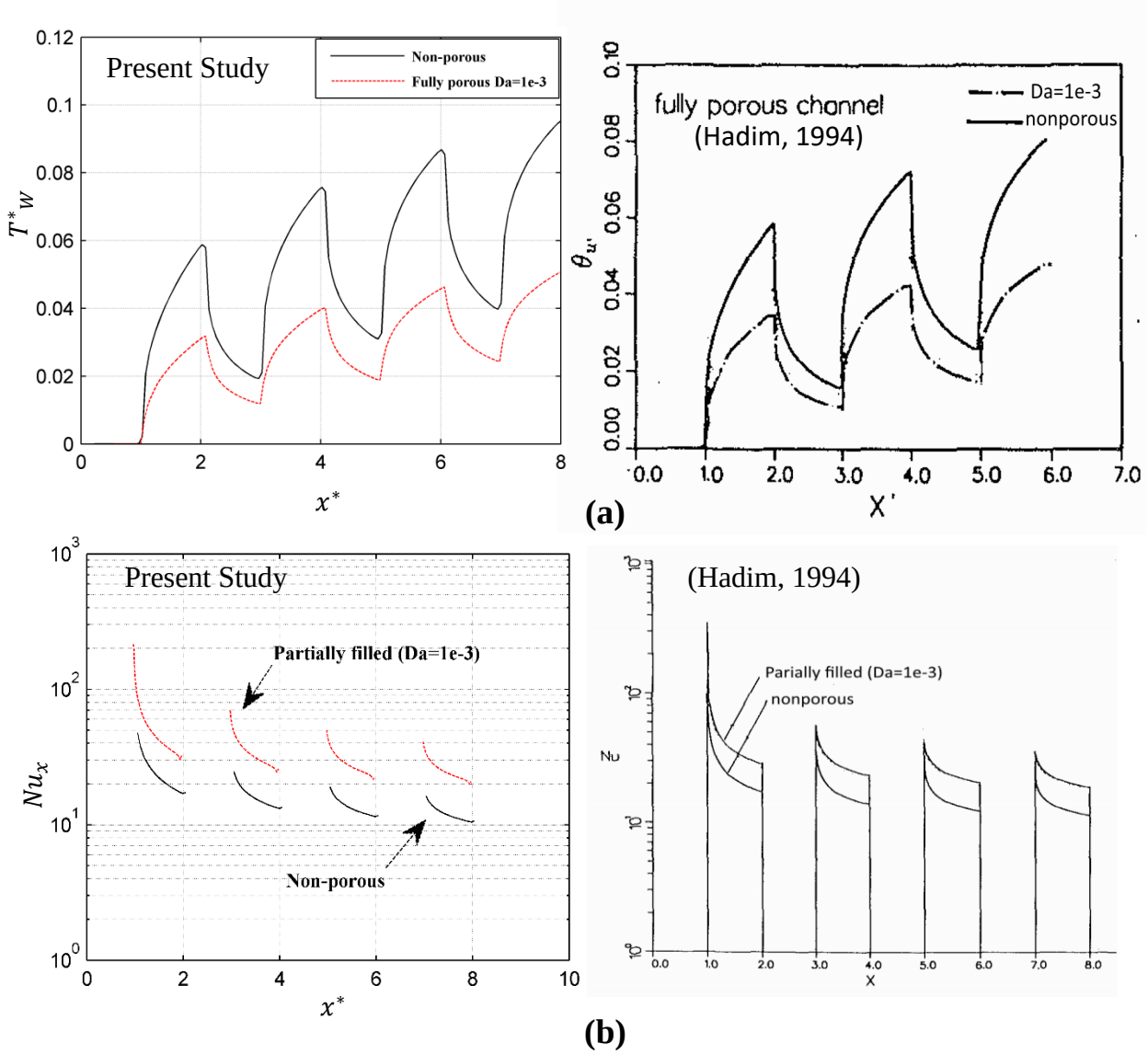

Figure 5. (a) Wall Temperature and **(b)** Local Nusselt number, Distribution along the Channel with and without MFI for Re= 250.

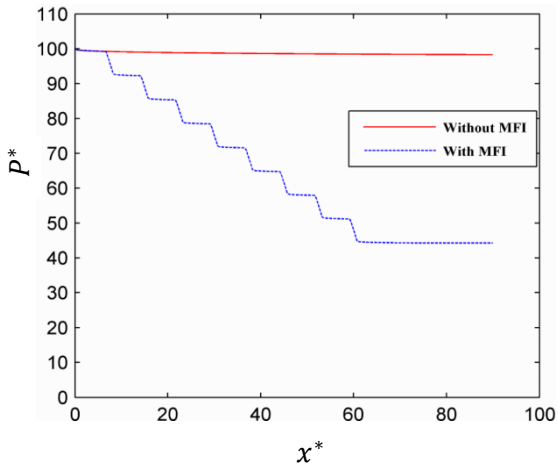

Figure 6. Local Dimensionless Pressure Distribution along the Channel with and without MFI for Re= 416.14, Gr=4.5×10^5.

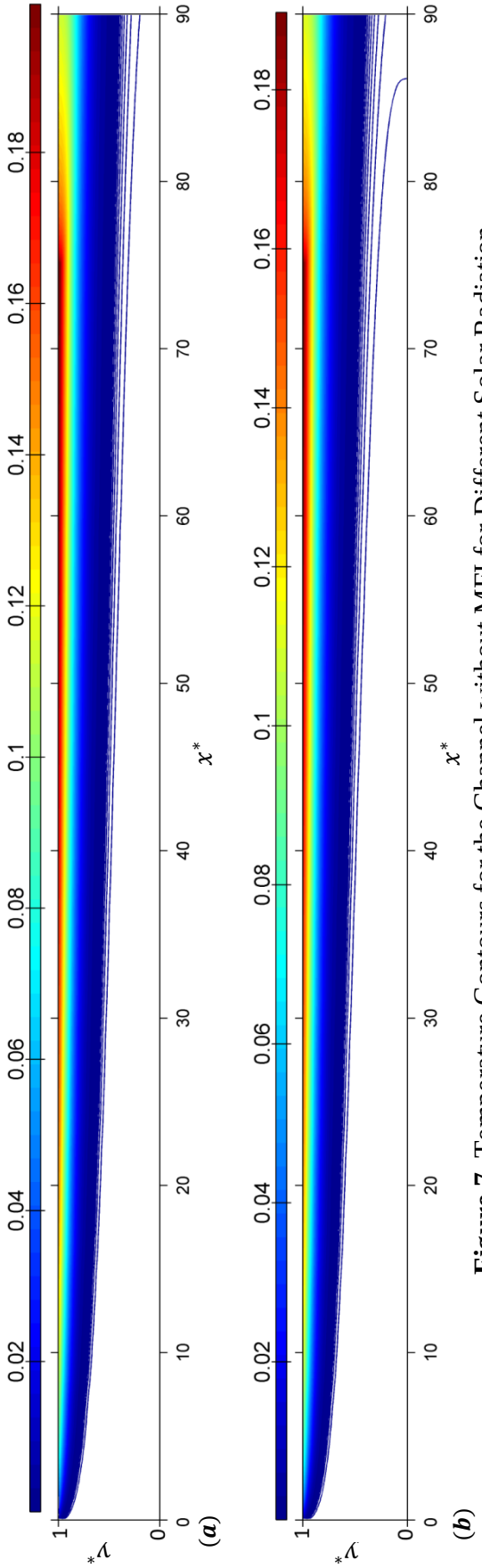

Figure 7. Temperature Contours for the Channel without MFI for Different Solar Radiation Intensity and Re=416.14, **(a)** I=515 W/m^2 & Gr = 5.15×10^5, **(b)** I=938 W/m^2 & Gr = 1.44×10^6,

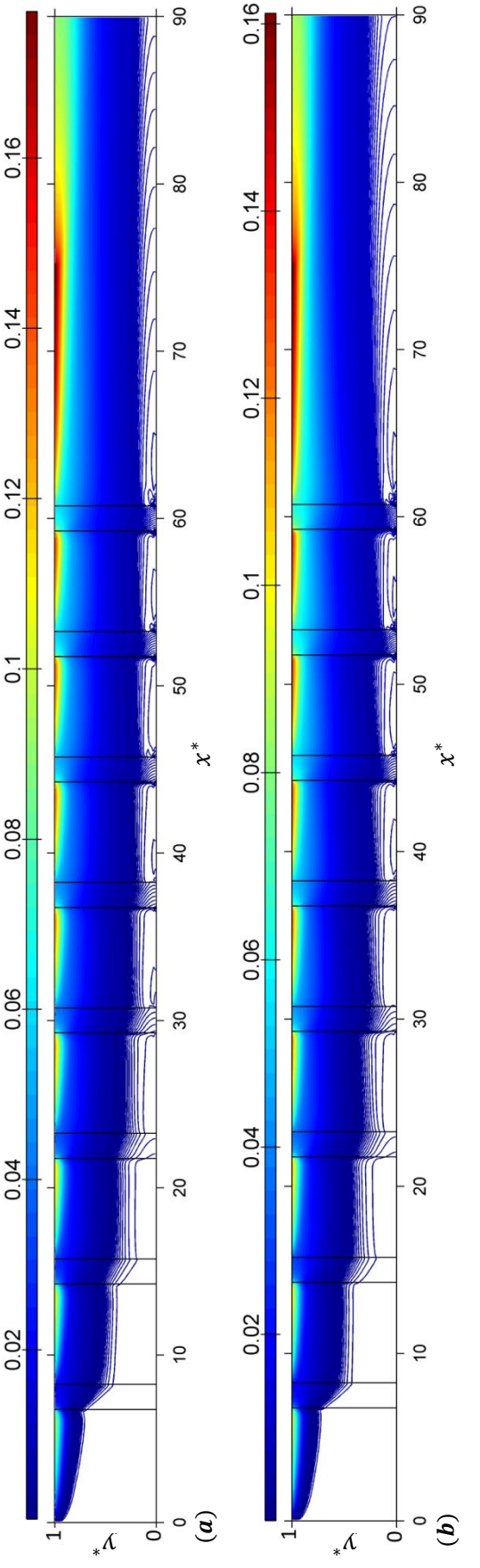

Figure 8. Temperature Contours for the Channel with MFI for Different Solar Radiation Intensity and Re=416.14, **(a)** I=515 W/m^2 & Gr = 5.15×10^5, **(b)** I=938 W/m^2 & Gr = 1.44×10^6,

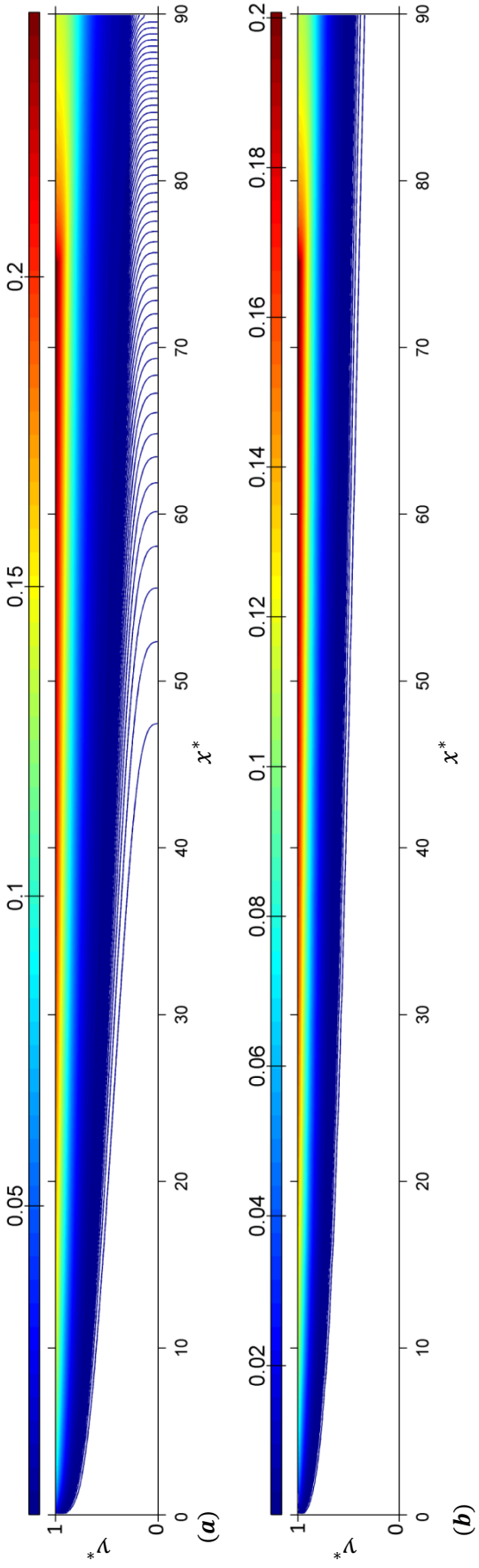

Figure 9. Temperature Contours for the Channel without MFI with Gr =4.5×10^5 and **(a)** Re =208, **(b)** Re = 624.22.

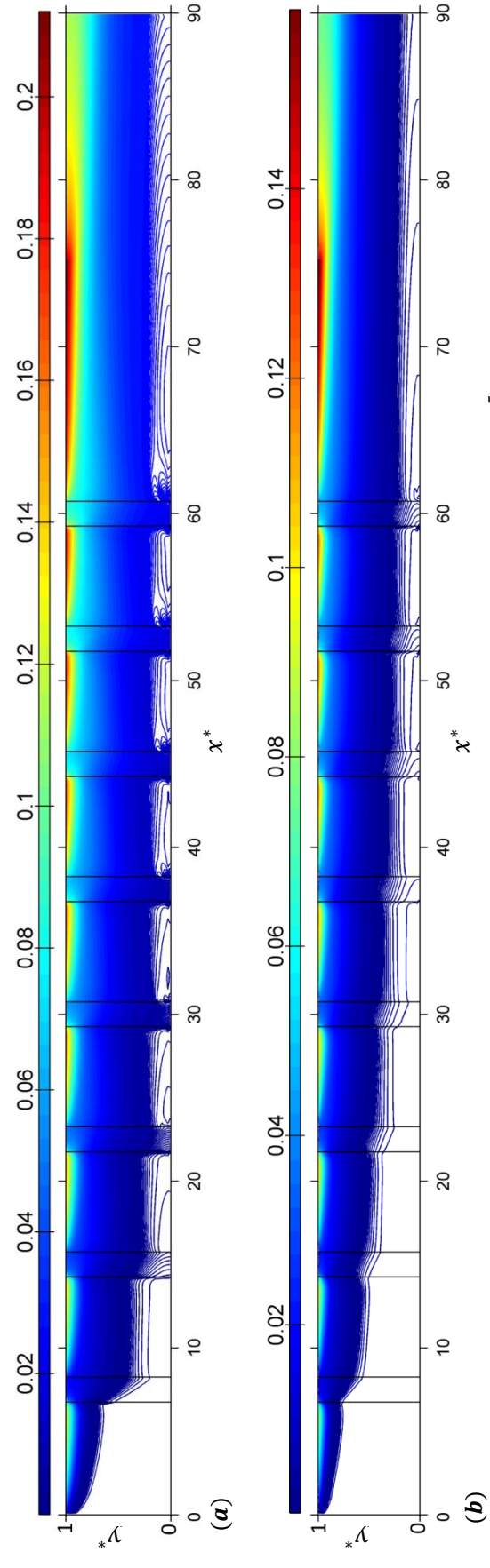

Figure 10. Temperature Contours for the Channel with MFI with Gr =4.5×10^5 and **(a)** Re =208, **(b)** Re = 624.22.

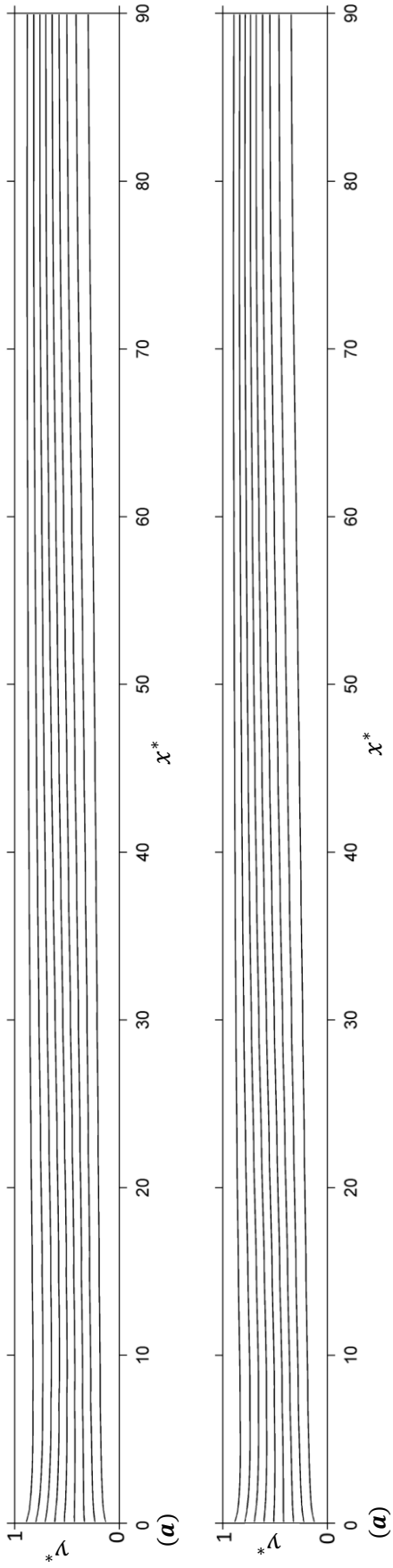

Figure 11. Streamlines for the Channel without MFI for Different Solar Radiation Intensity and Re=416.14, **(a)** I=515 W/m^2 & Gr = 5.15×10^5, **(b)** I=938 W/m^2 & Gr = 1.44×10^6,

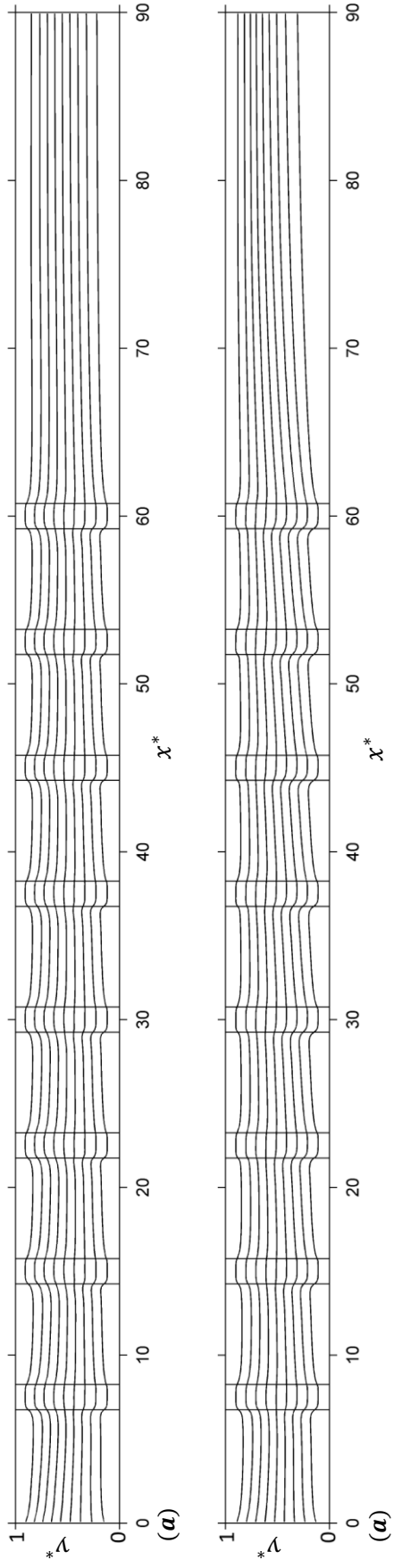

Figure 12. Streamlines for the Channel with MFI for Different Solar Radiation Intensity and Re=416.14, **(a)** I=515 W/m^2 & Gr = 5.15×10^5, **(b)** I=938 W/m^2 & Gr = 1.44×10^6,

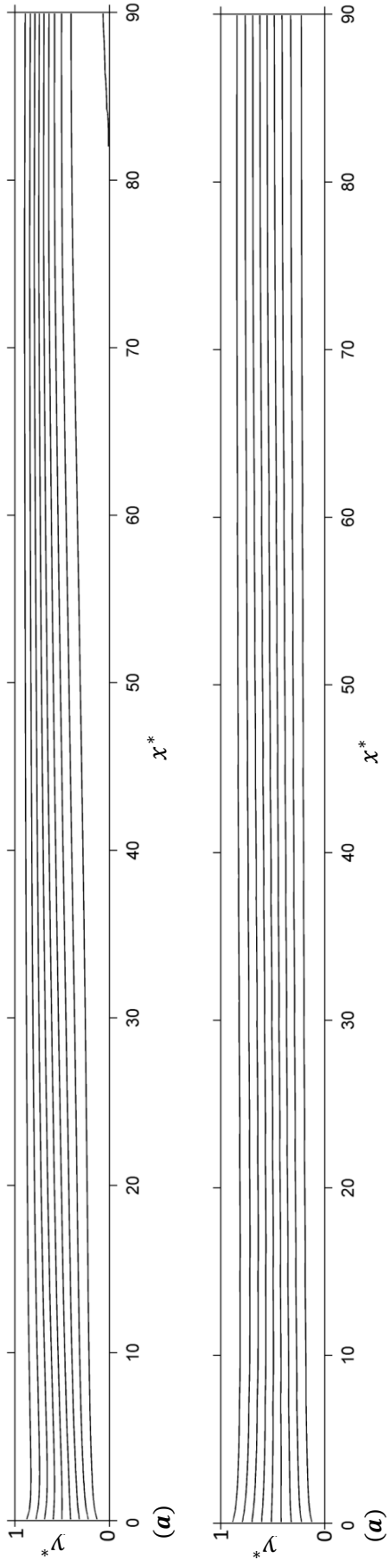

Figure 13. Streamlines for the Channel without MFI with Gr =4.5×10^5 and **(a)** Re =208, **(b)** Re = 624.22.

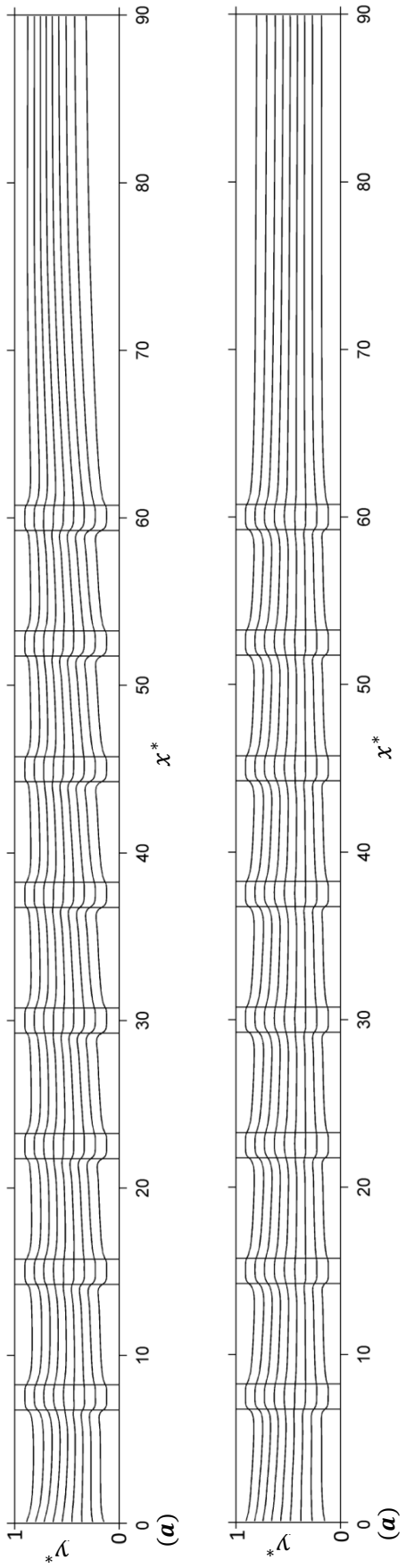

Figure 14. Streamlines for the Channel with MFI with Gr =4.5×10^5 and **(a)** Re =208, **(b)** Re = 624.22.

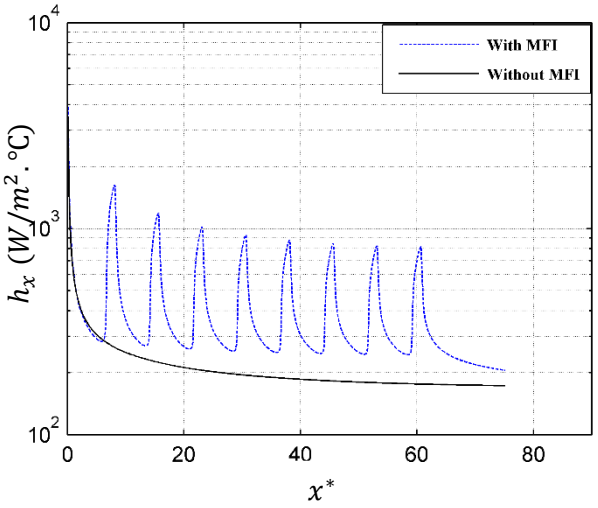

Figure 15. Local Convection Heat Transfer Coefficient Distribution along the Channel with and without MFI for Re= 208.07, Gr=4.5×10^5.

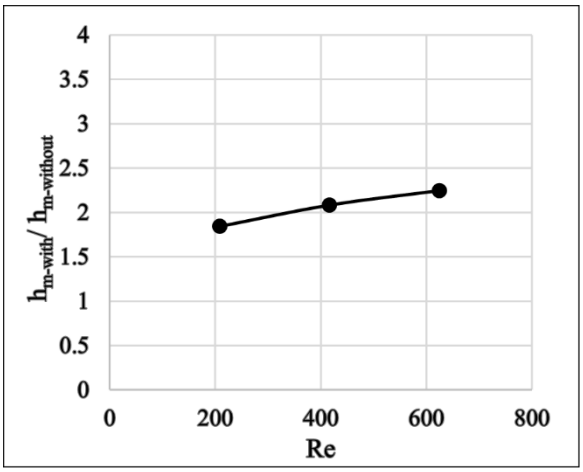

Figure 16. Variation of Heat Transfer Enhancement Factor with Different Reynolds No. and for Gr=4.5×10^5.

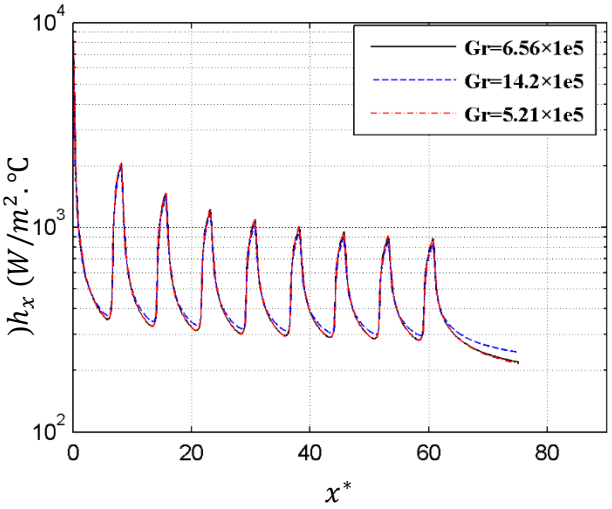

Figure 17. Local Convection Heat Transfer Coefficient Distribution along the Channel with MFI for Re= 416.14.

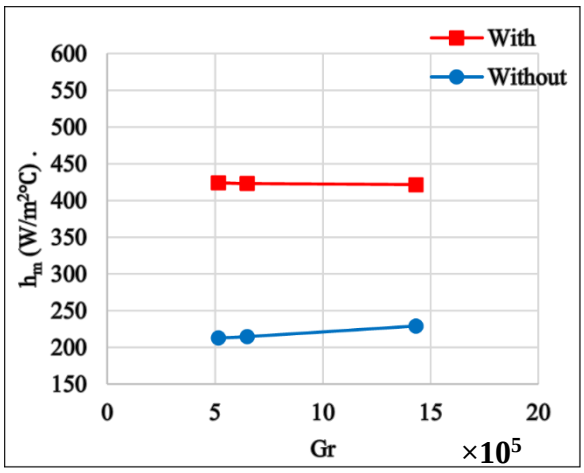

Figure 18. Mean Convection Heat Transfer Coefficient for the Channel with and without MFI for Re= 416.14.

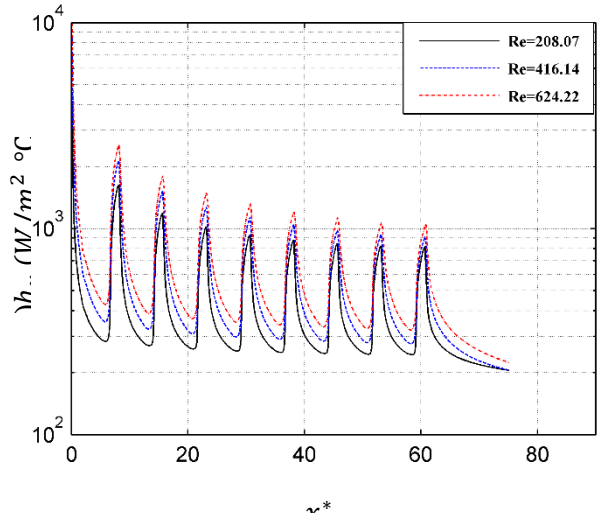

Figure 19. Local Convection Heat Transfer Coefficient Distribution along the Channel with Gr =4.5×10^5.

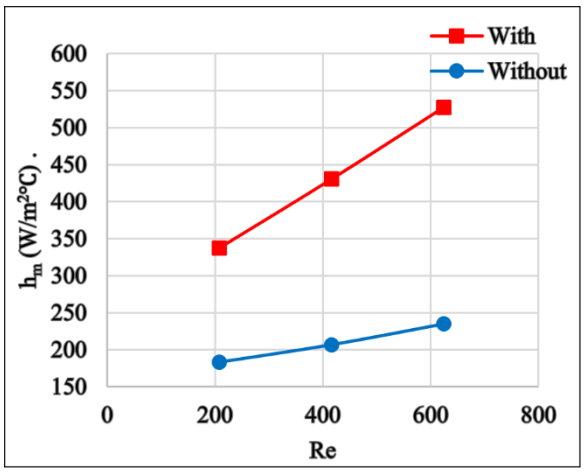

Figure 20. Mean Convection Heat Transfer Coefficient for the Channel with and without MFI for Gr =4.5×10^5.